coatings

MDPI

Article

Chemical Solution Deposition of La-Substituted $BiFe_{0.5}Sc_{0.5}O_3$ Perovskite Thin Films on Different Substrates

Diana Griesiute [1], Dovydas Karoblis [1], Lina Mikoliunaite [1,2], Aleksej Zarkov [1], Andrei N. Salak [3] and Aivaras Kareiva [1,*]

[1] Institute of Chemistry, Vilnius University, Naugarduko 24, LT-03225 Vilnius, Lithuania; diana.griesiute@chgf.vu.lt (D.G.); dovydas.karoblis@chgf.vu.lt (D.K.); lina.mikoliunaite@chf.vu.lt (L.M.); aleksej.zarkov@chf.vu.lt (A.Z.)

[2] Laboratory of Spectroelectrochemistry, Department of Organic Chemistry, Center for Physical Sciences and Technology, Sauletekio av. 3, LT-10257 Vilnius, Lithuania

[3] Department of Materials and Ceramic Engineering/CICECO, University of Aveiro, 3810-193 Aveiro, Portugal; salak@ua.pt

* Correspondence: aivaras.kareiva@chgf.vu.lt

Abstract: In the present work, polycrystalline $Bi_{0.67}La_{0.33}Fe_{0.5}Sc_{0.5}O_3$ thin films were synthesized using a simple and cost-effective chemical solution deposition process employing the spin coating technique. In order to check the feasibility of the fabrication of thin films on various types of substrates, the films were deposited on Pt-coated silicon, silicon, sapphire, corundum, fused silica and glass. Based on the results of thermogravimetric analysis of precursor and thermal stability study, it was determined that the optimal annealing temperature for the formation of perovskite structure is 600 °C. It was observed that the relative intensity of the pseudocubic peaks $(001)_p$ and $(011)_p$ in the XRD patterns is influenced by the nature of substrates, suggesting that the formed crystallites have some preferred orientation. Roughness of the films was determined to be dependent on the nature of the substrate.

Keywords: $Bi_{1-x}La_xFe_{0.5}Sc_{0.5}O_3$; perovskite; thin film; chemical solution deposition

Citation: Griesiute, D.; Karoblis, D.; Mikoliunaite, L.; Zarkov, A.; Salak, A.N.; Kareiva, A. Chemical Solution Deposition of La-Substituted $BiFe_{0.5}Sc_{0.5}O_3$ Perovskite Thin Films on Different Substrates. *Coatings* **2021**, *11*, 307. https://doi.org/10.3390/coatings11030307

Academic Editor: Christian Mitterer

Received: 15 February 2021
Accepted: 4 March 2021
Published: 8 March 2021

1. Introduction

In recent decades multiferroic materials have attracted huge scientific and technological interest due to their unique physical properties. The coexistence of intimately coupled ferroic orders makes it possible to influence the state of the material by applying external electrical or magnetic fields [1]. A number of families of oxide materials with magnetic, ferroelectric, and ferroelastic properties and their combinations are composed of three-dimensional chains of metal–oxygen octahedra [2]. The perovskite family is probably the most famous in this respect [3].

Bismuth ferrite (BFO, $BiFeO_3$) is one of the most known multiferroic materials with a perovskite crystal structure [4]. This perovskite demonstrates outstanding physical properties such as large remnant polarization (~100 μC/cm²), high Curie temperature (T_C ~ 1100 K) and high Néel temperature (T_N ~643 K) [5,6]. Its direct band gap (E_g) of around 2.2–2.8 eV allows for efficient light absorption in the visible spectral range [7]. One of the approaches commonly employed for the tuning of magnetic, electrical, structural and optical properties of BFO considers a partial substitution of Bi^{3+} and/or Fe^{3+} ions by isovalent or aliovalent ions [8–10]. The remarkable BFO derivative, which is in fact A and B co-substituted BFO, is the $Bi_{1-x}La_xFe_{0.5}Sc_{0.5}O_3$ perovskite system [11,12]. In the bulk form of this material, the room temperature compositional crossover from the antipolar phase, the incommensurate modulation of displacements of Bi/La and oxygen of which is de-

scribed by the *Imma*(00γ)s00 superspace group [13] to the nonpolar *Pnma* phase [14], occurs in the narrow range between x = 0.33 and 0.34 with no phase coexistence [15]. This very narrow compositional range is of a great interest, since it corresponds to a solid solution with the maximal lattice-magnetic coupling effect expected, since $T_C \approx T_N$ [15]. It is known that the perovskites phases of the $Bi_{1-x}La_xFe_{0.5}Sc_{0.5}O_3$ system ($x < 0.80$) can be prepared in forms of ceramics only using high-pressure synthesis [13–15], and they are metastable at ambient pressure. It should be noticed that while $Bi_{0.67}La_{0.33}Fe_{0.5}Sc_{0.5}O_3$ and $Bi_{0.66}La_{0.34}Fe_{0.5}Sc_{0.5}O_3$ in bulk form have been studied [11,12,15], to the best of our knowledge there are no reports on the synthesis and investigation of physical properties of their thin films.

Fabrication of multiferroic materials in the form of 2D nanostructures is of particular technological importance for the development and miniaturization of electronic devices [16,17]. Moreover, the aspects such as preferred orientation or surface strain can be considered as an additional powerful tool, allowing the physical properties of the materials to be tuned [18,19]. For the fabrication of multicomponent oxide thin films, various deposition approaches, including vacuum-based and non-vacuum based techniques, can be successfully employed [20–24]. It is well known that for some advanced deposition methods, such as metal organic chemical solution deposition, the precise stoichiometric control in multicomponent systems is a very challenging task because of different volatility of precursors, different deposition rates, etc. [25,26]. The methods based on physical vapor deposition also suffer from the deviation from desired product stoichiometry [27]. In this light, chemical solution deposition can be considered as a reasonable choice for production of mixed metal oxide films. This method is remarkable due to its low cost, simplicity, good mixing of starting materials at the molecular level and ease of processing for large-area wafers. Excellent stoichiometry control of the end product is easily achieved by the use of appropriate amounts of starting materials. All these features allow homogeneous and single-phase products to be obtained [28–30].

This study is the first step towards the systematic investigation of physical properties of $Bi_{1-x}La_xFe_{0.5}Sc_{0.5}O_3$ thin films. The main objective of this work was to develop a simple and reliable procedure for the deposition of $Bi_{0.67}La_{0.33}Fe_{0.5}Sc_{0.5}O_3$ 2D nanostructures. Additionally, this work was aimed at checking the feasibility of preparation of the $Bi_{0.67}La_{0.33}Fe_{0.5}Sc_{0.5}O_3$ thin films on different kinds of substrates (monocrystalline, polycrystalline, amorphous, transparent and conductive) for further characterization of physical properties. For this reason, soda lime glass, polycrystalline Al_2O_3, fused silica, monocrystalline silicon wafer, sapphire and Pt-coated silicon ($Pt/TiO_2/SiO_2/Si$) substrates were selected. The influence of the substrate on structural properties and morphology of deposited thin films was investigated.

2. Materials and Methods

2.1. Preparation of Precursor Solution

The synthesis of precursor solution was performed on the basis of a previously reported procedure [31]. An appropriate amount of scandium oxide (Sc_2O_3, abcr, 99.9%) was dissolved in boiling concentrated nitric acid and evaporated to dryness. The obtained scandium salt was further dissolved in a certain volume of 2-methoxyethanol ($C_3H_8O_2$, Sigma-Aldrich, Darmstadt, Germany, 99.8%). Metal nitrate hydrates $La(NO_3)_3{\cdot}6H_2O$ (Roth, Karlsruhe, Germany, 99.99%), $Bi(NO_3)_3{\cdot}5H_2O$ (Roth, 98%) and $Fe(NO_3)_3{\cdot}9H_2O$ (Sigma-Aldrich, 98%) were added to the above solution according to the stoichiometry of the final product ($Bi_{0.67}La_{0.33}Fe_{0.5}Sc_{0.5}O_3$). A certain amount of acetic anhydride ($(CH_3CO)_2O$, Sigma-Aldrich, ≥99%) was then added to the prepared mixture; the volume ratio of 2-methoxyethanol and acetic anhydride was 3:1. The total concentration of metal ions in the obtained clear precursor solution was 0.25 M. Thermogravimetric analysis and elemental analysis of metal nitrates by means of inductively coupled plasma optical emission spectrometry (ICP-OES) were performed prior synthesis in order to estimate the actual metal

content. Hereafter in the text, the chemical formula ($Bi_{0.67}La_{0.33}Fe_{0.5}Sc_{0.5}O_3$) will be abbreviated as BLFSO.

2.2. Deposition of Thin Films

Multilayered thin films were prepared on Pt-coated silicon ($Pt/TiO_2/SiO_2/Si$, UniversityWafer, South Boston, MA, United States), silicon (CrysTec, Berlin, Germany), R-cut sapphire (CrysTec), polycrystalline corundum (MTI, Richmond, CA, United States), fused silica (Altechna, Vilnius, Lithuania) and glass (Roth) substrates by the spin coating technique using a SCS P6700 spin coater. Prior to deposition, the substrates were cleaned with a concentrated sulfuric acid and hydrogen peroxide (30%) mixture followed by washing with deionized water and isopropanol. Several drops of precursor solution were placed onto substrates and spin coated for 30 s at 3000 rpm. The as-deposited wet films were dried on a hot plate in a two-step manner: 5 min at 90 °C followed by 5 min at 270 °C. The complete cycle was repeated a certain number of times prior to a final annealing in a muffle furnace at different temperatures for 2 h (the heating rate was 1 °C/min). All films were deposited using the same precursor solution on the same day. An aliquot of precursor solution was evaporated and annealed under identical conditions in order to obtain BLFSO powders for comparison. A schematic representation of the deposition procedure is shown in Figure 1.

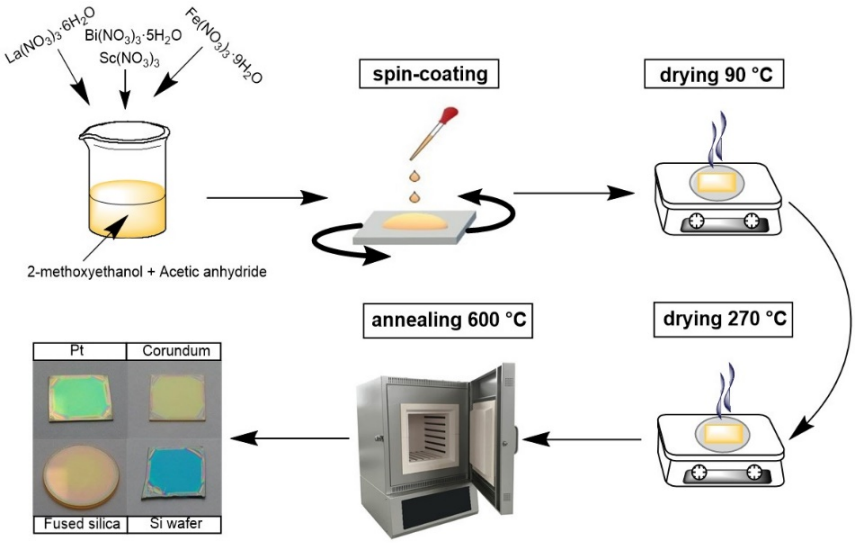

Figure 1. Schematic representation of the synthesis of BLFSO thin films and optical photographs of the films deposited on $Pt/TiO_2/SiO_2/Si$, corundum, silicon and fused silica substrates.

2.3. Characterization

The thermal decomposition of dried precursor solution was analyzed by thermogravimetry and differential scanning calorimetry (TG–DSC) using a Perkin Elmer STA 6000 simultaneous thermal analyzer. A dried sample of about 5–10 mg was heated from 25 to 900 °C at a heating rate of 5 °C/min in dry flowing air (20 mL/min). The crystal structure of the obtained samples was investigated by X-ray diffraction (XRD) using a PANalytical X'Pert powder diffractometer (Theta-Omega goniometer, Malvern Panalytical, Malvern, UK, Ni-filtered Cu Kα radiation, PIXcel^{1D} detector, Malvern Panalytical, Malvern, UK, tube settings 45 kV, 40 mA). The deposited films were measured in grazing incidence X-ray diffraction (GIXRD) mode using a multi-purpose sample stage. The XRD patterns were collected with a grazing angle of 2° in the range from 20 to 80 degrees with a step of 0.02° and a counting time of about 7 s per step. Prior to each measurement, the substrate position was aligned against the direct beam by means of the omega angle correction. The

XRD measurements of the powder samples were performed using a spinner sample stage (Bragg-Brentano geometry, a 2θ angular range of 20°–80°, step 0.02°, 0.5 s per step, a sample rotation of 4 s^{-1}). The obtained XRD data were treated using the PANalytical HighScore 5.0 package. The morphology of the films was characterized using a Hitachi SU-70 scanning electron microscope (SEM) (Hitachi, Tokyo, Japan). For the surface characterization of the deposited films, a BioScope Catalyst atomic force microscope (AFM) from Bruker (BioscopeII/Catalyst, Karlsruhe, Germany) was used. The peak force tapping mode was applied using a ScanAsyst-Air silicon probe (nominal tip spring constant 0.4 N/m, scan rate 0.5 Hz). Two types of images were recorded: 20 μm × 20 μm and 5 μm × 5 μm.

3. Results and Discussion

The thermal decomposition behavior of dried BLFSO precursor solution was investigated by simultaneous TG–DSC measurements (Figure 2) in order to determine the annealing temperature range suitable for the formation of a perovskite structure. Three main steps in the thermal degradation process can be seen. Insignificant weight loss accompanied by a weak endothermic signal can be noticed at low temperatures around 100 °C. This process could be ascribed to the removal of residual water and organic solvent. Further considerable weight loss corresponds to the decomposition of nitrates and organic species. The constant mass of the residual was observed at temperatures above 600 °C; therefore, this temperature was chosen for the final thermal treatment of the deposited films. Moreover, a higher annealing temperature would lead to the melting of glass substrates, whereas for correct comparison of the films, annealing temperature should be the same for all substrates. Based on a TG curve, the total weight loss was calculated to be 57%.

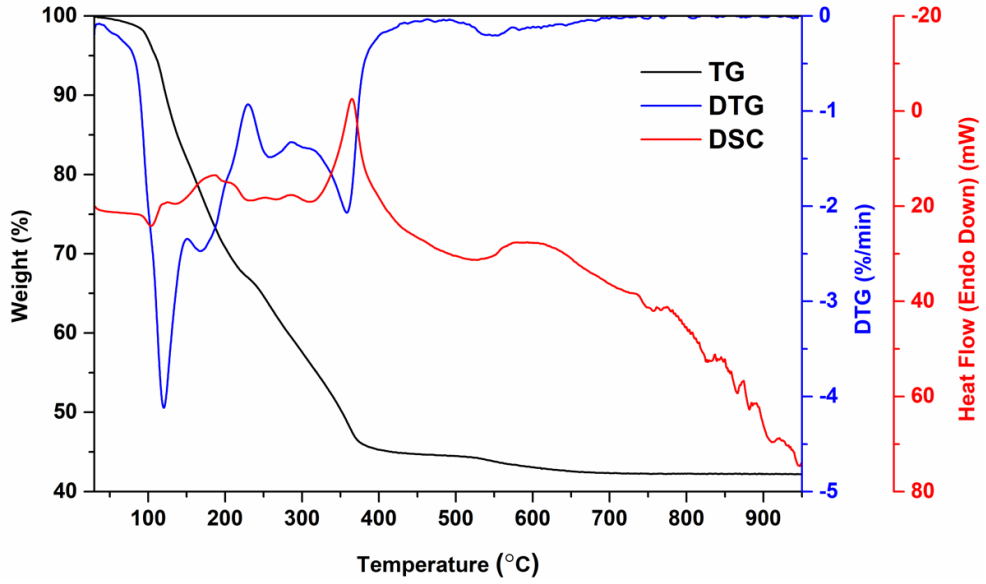

Figure 2. TG–DTG–DSC curves of dried Bi–La–Fe–Sc–O precursor solution.

The phase crystallinity and purity of all synthesized samples were characterized by means of XRD analysis. Figure 3 represents the XRD patterns of the BLFSO coatings deposited on different substrates and annealed at 600 °C for 2 h. It is evident that the crystalline phase was formed after annealing regardless of the nature of the substrate. Intense and well-resolved diffraction peaks corresponding to the pseudocubic perovskite structure [15] could be seen in all the XRD patterns. In the case of $Pt/TiO_2/SiO_2/Si$, silicon, sapphire and corundum, the diffraction reflections arising from the substrates were also seen.

The broad diffraction peaks indicate the nanocrystalline nature of the films, which was expected after crystallization at relatively low temperatures. The obtained results suggest that proposed deposition procedure is suitable for the fabrication of perovskite thin films on monocrystalline, polycrystalline, amorphous, transparent and conductive substrate, which provides broad possibilities and flexibility in terms of the further investigation of the physical properties of this material.

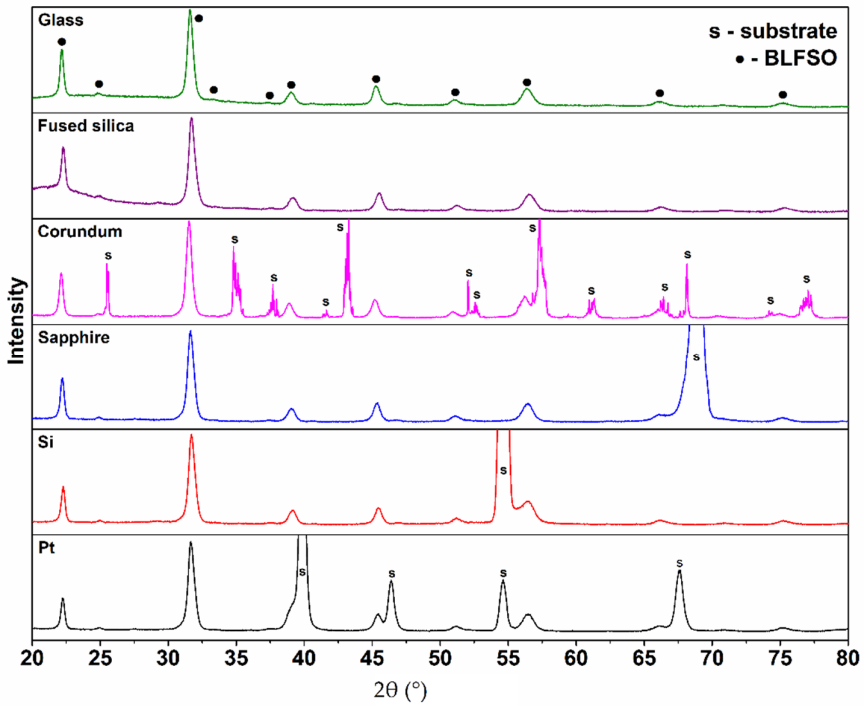

Figure 3. XRD patterns of the BLFSO films processed at 600 °C on different substrates.

It is well known that high annealing temperatures may lead to the formation of dense, well-crystallized films. However, the limitations caused by the metastable nature of bulk BLFSO do not suggest high-temperature processing. For this reason, some of the synthesized films were additionally annealed at different temperatures in order to determine the limiting annealing conditions. The XRD patterns of BLFSO films deposited on $Pt/TiO_2/SiO_2/Si$ substrate and annealed at 550–800 °C are depicted in Figure 4.

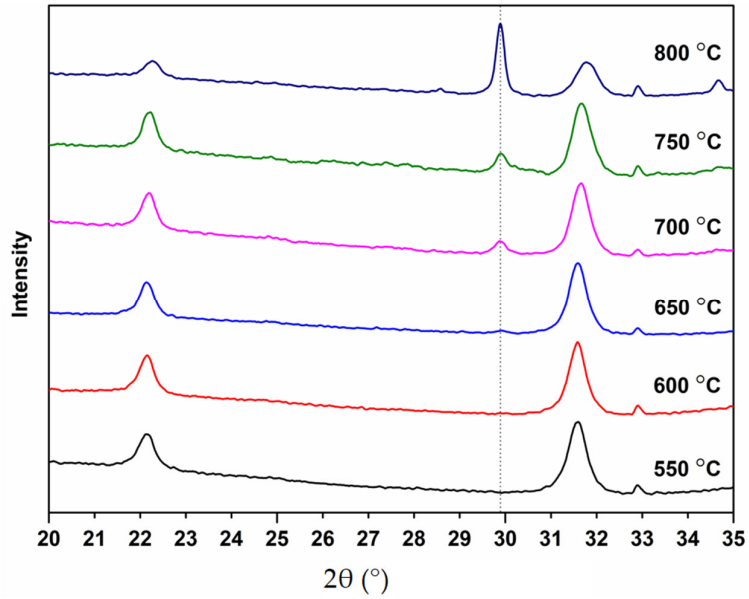

Figure 4. XRD patterns of the BLFSO films annealed at different temperatures ($Pt/TiO_2/SiO_2/Si$ substrate).

XRD data were collected in the 20–35 2θ range, which contained the most intense peaks and where impurity phases such as Bi_2O_3, $Bi_2Fe_4O_9$ or $Bi_{25}FeO_{39}$ are usually detected [32,33]. It could be seen that there were no changes in the XRD patterns when the temperature was increased up to 600 °C. After annealing at 650 °C, a low intensity diffraction peak at ca. 30° appeared. The intensity of this peak gradually increased with an increase of annealing temperature. At the same time, the intensity of the most intense peak of the perovskite phase (at around 31.6°) decreased, and the peak shifted towards a higher 2θ region. One more peak, located at around 34.7°, arose after annealing at temperatures above 700 °C. The observed annealing-induced changes indicated decomposition of the perovskite phase and suggested that 600 °C was the most suitable annealing temperature. In order to reveal possible influence of the substrates on crystal structure, strain and/or texture of the deposited films, the full width at half maximum (FWHM) values for the two most intense diffraction reflections $(001)_p$ and $(011)_p$ (in pseudocubic perovskite lattice) located at ca. 22.3° and 31.7° were estimated and compared with the respective values for the powder obtained by calcination of the precursor solution at 600 °C (Figure 5).

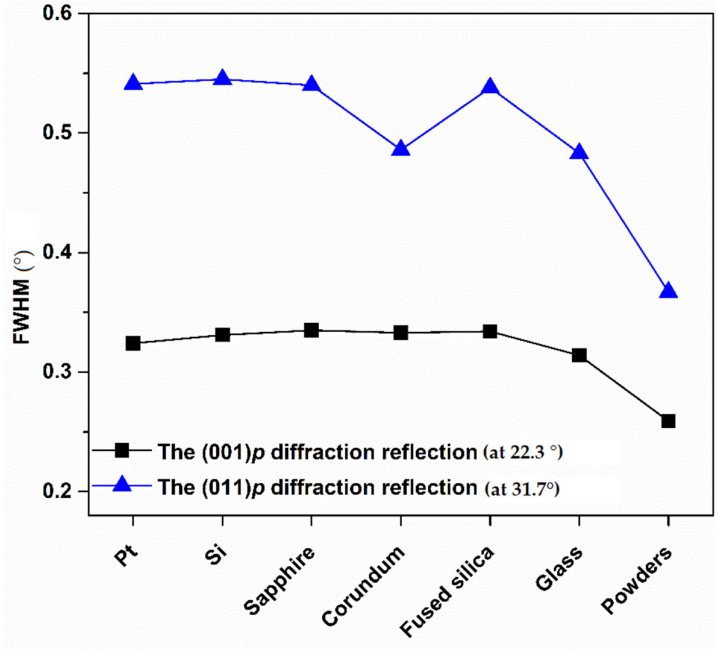

Figure 5. FWHM of the $(001)_p$ and $(011)_p$ reflections for the films fabricated on different substrates.

Although in the vicinity of the compositional crossover from the *Imma*(00γ)s00 phase to the non-polar *Pnma* phase, the symmetry of the primitive perovskite cell of the $Bi_{1-x}La_xFe_{0.5}Sc_{0.5}O_3$ perovskites is near cubic [15], a transition between these phases could be detected by variation in the FWHM value of the most characteristic diffractions reflections. As seen from Figure 5, for each particular substrate, FWHM of the $(001)_p$ reflection was regularly smaller than that of the $(011)_p$ reflection, suggesting that all the obtained films were of the same symmetry.

The $(011)_p$ to $(001)_p$ intensities ratios for different substrates are shown in Figure 6. It is seen that intensity ratios were clearly dependent on the nature of the substrates. This value was estimated for the Pt substrate to be about 4.7. The lowest values were obtained for the amorphous substrates; for instance, it was only about 2.6 for the film on glass substrate. For the powder prepared from the precursor solution, this value was about 3.0.

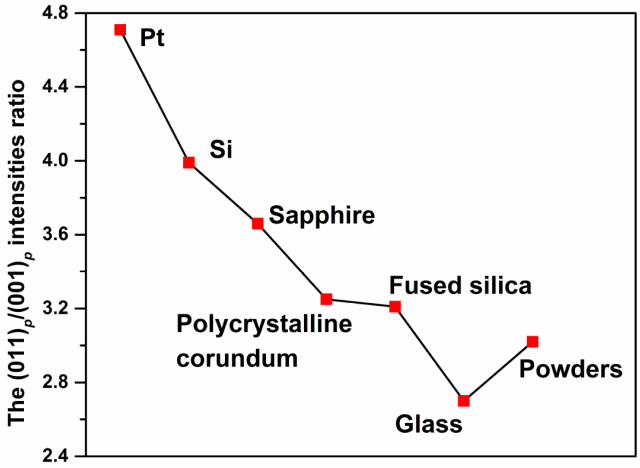

Figure 6. Ratio of the intensities of the $(011)_p$ and $(001)_p$ reflections in XRD patterns of the BLFSO films fabricated on different substrates. The point corresponding to the respective value for the powder sample is shown for comparison.

The microstructure of the BLFSO films was examined by SEM. The most representative plane views of the films deposited on $Pt/TiO_2/SiO_2/Si$, silicon, sapphire and fused silica followed by annealing at 600 °C are given in Figure 7. The morphology of the films fabricated on all types of substrates was very similar. The obtained films were uniform but not absolutely dense: some pores could be observed. Thickness of the films was determined by SEM analysis of the cross-section. It was found that single-layered film obtained by one deposition cycle was about 50 nm thick. Moreover, the thickness of the films was independent of the type of substrate.

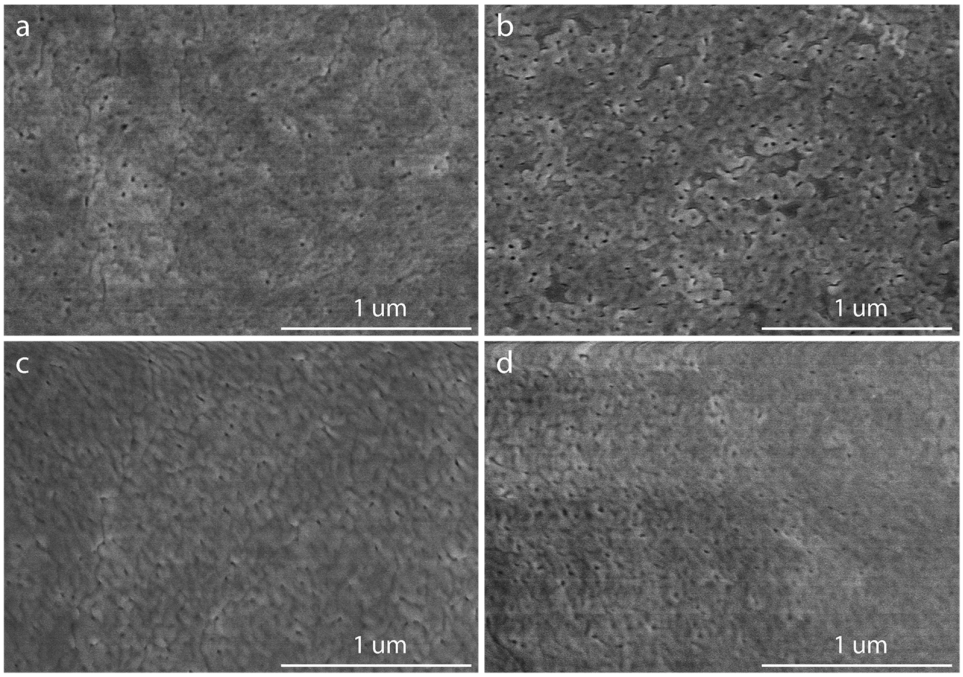

Figure 7. Plane view SEM images of the BLFSO films deposited on $Pt/TiO_2/SiO_2/Si$ (**a**), silicon (**b**), sapphire (**c**) and fused silica (**d**).

Figure 8 demonstrates 2D AFM images of the BLFSO films deposited on different substrates. The obtained images are in good agreement with the obtained SEM micrographs and confirm the presence of nanodimensional pores. The roughness of the films and non-coated substrates was estimated by calculation of the root mean square of height values (RMS), which are summarized in Table 1. The RMS values were calculated for the relatively large (20 μm × 20 μm) and the relatively small (5 μm × 5 μm) areas; the obtained results were in good agreement. It is seen that the roughness of the film was higher than that of uncoated substrate with an exception for mechanically polished corundum, which possessed a relatively rough initial surface. The RMS values varied in the range from 3.1 to 7.3 nm, and the highest roughness was observed for the $Pt/TiO_2/SiO_2/Si$ substrate and the lowest for the fused silica one.

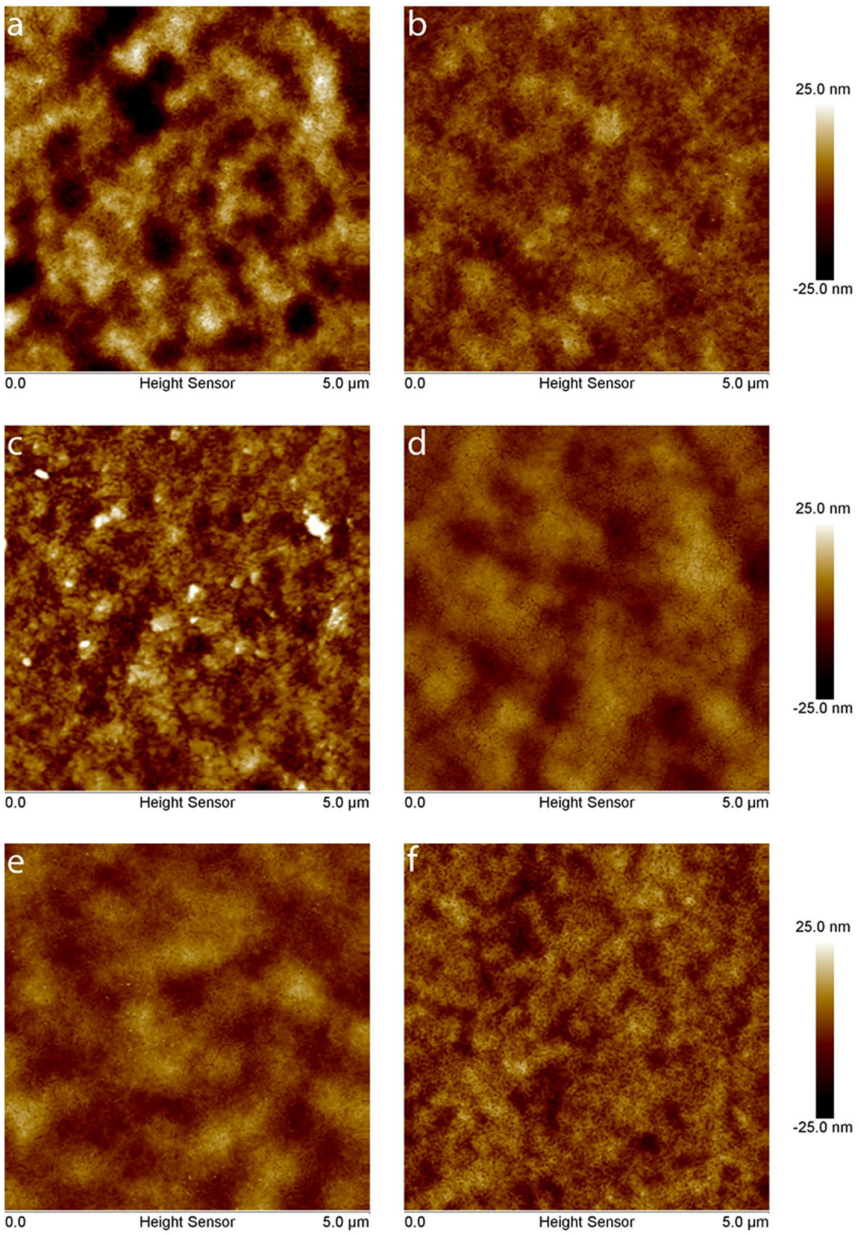

Figure 8. AFM images of the BLFSO films processed at 600 °C on Pt/TiO_2/SiO_2/Si (**a**), silicon (**b**), sapphire (**c**), corundum (**d**), fused silica (**e**) and glass (**f**).

Table 1. Roughness of selected substrates and films calculated as RMS.

Substrate	Roughness of Substrate, nm	Roughness of Film on the Respective Substrate, nm
Pt/TiO_2/SiO_2/Si, Si/SiO_2	4.2 ± 0.1	7.3 ± 0.8
Silicon	0.6 ± 0.3	3.8 ± 0.1
Sapphire	1.2 ± 0.2	5.8 ± 0.9
Corundum	9.2 ± 2	4.8 ± 0.2
Fused silica	0.8 ± 0.1	3.1 ± 0.5
Glass	1.1 ± 0.1	4.2 ± 0.3

4. Conclusions

Polycrystalline $Bi_{0.67}La_{0.33}Fe_{0.5}Sc_{0.5}O_3$ thin films were successfully fabricated by chemical solution deposition using a spin coating technique. Multi-layered films with perovskite structure were prepared on $Pt/TiO_2/SiO_2/Si$, silicon, sapphire, corundum, fused silica and glass substrates after annealing at 600 °C. Processing at higher temperatures resulted in the decomposition of the perovskite phase. The films were found to be of the same crystal symmetry regardless of the substrate used. At the same time, the relative intensity of the pseudocubic peaks $(001)_p$ and $(011)_p$ in XRD patterns was rather different for the films on different substrates, suggesting that the perovskite crystallites have some preferred orientation. The roughness of the films varied in the range from 3.1 to 7.3; the highest roughness was observed for the $Pt/TiO_2/SiO_2/Si$ substrate and the lowest for the fused silica substrate.

Author Contributions: Conceptualization, A.N.S. and A.Z.; methodology, A.Z.; formal analysis, D.G., D.K., L.M., A.N.S., and A.Z.; investigation, D.G., D.K., L.M., A.N.S., and A.Z.; resources, A.K.; writing—original draft preparation, D.G.; writing—review and editing, A.K.; visualization, D.G.; supervision, A.K.; All authors have read and agreed to the published version of the manuscript.

Funding: This work was supported by a Research grant BUNACOMP (No. S-MIP-19-9) from the Research Council of Lithuania (LMTLT). The research performed in the University of Aveiro was developed within the scope of the project CICECO-Aveiro Institute of Materials, UIDB/50011/2020 and UIDP/50011/2020, financed by national funds through the FCT/MEC and when appropriate co-financed by FEDER under the PT2020 Partnership Agreement.

Institutional Review Board Statement: Not applicable.

Informed Consent Statement: Not applicable.

Data Availability Statement: Data is contained within the article or supplementary material.

Conflicts of Interest: The authors declare no conflict of interest.

References

1. Vopson, M.M. Fundamentals of multiferroic materials and their possible applications. *Crit. Rev. Solid State Mater. Sci.* **2015**, *40*, 223–250, doi:10.1080/10408436.2014.992584.
2. Lu, C.; Wu, M.; Lin, L.; Liu, J.-M. Single-phase multiferroics: New materials, phenomena, and physics. *Natl. Sci. Rev.* **2019**, *6*, 653–668, doi:10.1093/nsr/nwz091.
3. Liu, H.; Yang, X. A brief review on perovskite multiferroics. *Ferroelectrics* **2017**, *507*, 69–85, doi:10.1080/00150193.2017.1283171.
4. Catalan, G.; Scott, J.F. Physics and applications of bismuth ferrite. *Adv. Mater.* **2009**, *21*, 2463–2485, doi:10.1002/adma.200802849.
5. Molak, A.; Mahato, D.K.; Szeremeta, A.Z. Synthesis and characterization of electrical features of bismuth manganite and bismuth ferrite: Effects of doping in cationic and anionic sublattice: Materials for applications. *Prog. Cryst. Growth Charact. Mater.* **2018**, *64*, 1–22, doi:10.1016/j.pcrysgrow.2018.02.001.
6. Chen, L.; Cheng, Z.; Xu, W.; Meng, X.; Yuan, G.; Liu, J.; Liu, Z. Electrical and mechanical switching of ferroelectric polarization in the 70 nm $BiFeO_3$ film. *Sci. Rep.* **2016**, *6*, 19092, doi:10.1038/srep19092.
7. Ceballos-Sanchez, O.; Sanchez-Martinez, A.; Flores-Ruiz, F.J.; Huerta-Flores, A.M.; Torres-Martínez, L.M.; Ruelas, R.; García-Guaderrama, M. Study of $BiFeO_3$ thin film obtained by a simple chemical method for the heterojunction-type solar cell design. *J. Alloys Compd.* **2020**, *832*, 154923, doi:10.1016/j.jallcom.2020.154923.
8. Catalano, M.R.; Spedalotto, G.; Condorelli, G.G.; Malandrino, G. MOCVD growth of perovskite multiferroic $BiFeO_3$ films: The effect of doping at the A and/or B sites on the structural, morphological and ferroelectric properties. *Adv. Mater. Interfaces* **2017**, *4*, 1601025, doi:10.1002/admi.201601025.
9. McLeod, J.A.; Pchelkina, Z.V.; Finkelstein, L.D.; Kurmaev, E.Z.; Wilks, R.G.; Moewes, A.; Solovyev, I.V.; Belik, A.A.; Takayama-Muromachi, E. Electronic structure of $BiMO_3$ multiferroics and related oxides. *Phys. Rev. B* **2010**, *81*, 144103, doi:10.1103/PhysRevB.81.144103.
10. Arnold, D.C. Composition-driven structural phase transitions in rare-earth-doped $BiFeO_3$ ceramics: A review. *IEEE Trans. Ultrason. Ferroelectr. Freq. Control* **2015**, *62*, 62–82, doi:10.1109/TUFFC.2014.006668.
11. Fertman, E.L.; Fedorchenko, A.V.; Khalyavin, D.D.; Salak, A.N.; Baran, A.; Desnenko, V.A.; Kotlyar, O.V.; Cizmar, E.; Feher, A.; Syrkin, E.S.; et al. Multiferroic $Bi_{0.65}La_{0.35}Fe_{0.5}Sc_{0.5}O_3$ perovskite: Magnetic and thermodynamic properties. *J. Magn. Magn. Mater.* **2017**, *429*, 177–181, doi:10.1016/j.jmmm.2017.01.037.

12. Fedorchenko, A.V.; Fertman, E.L.; Desnenko, V.A.; Kotlyar, O.V.; Cizmar, E.; Shvartsman, V.V.; Lupascu, D.C.; Salamon, S.; Wende, H.; Salak, A.N.; et al. Magnetic properties of the $Bi_{0.65}La_{0.35}Fe_{0.5}Sc_{0.5}O_3$ perovskite. *Acta Phys. Pol. A* **2017**, *131*, 1069–1071, doi:10.12693/APhysPolA.131.1069.
13. Khalyavin, D.D.; Salak, A.N.; Lopes, A.B.; Olekhnovich, N.M.; Pushkarev, A.V.; Radyush, Y.V.; Fertman, E.L.; Desnenko, V.A.; Fedorchenko, A.V.; Manuel, P.; et al. Magnetic structure of an incommensurate phase of La-doped $BiFe_{0.5}Sc_{0.5}O_3$: Role of antisymmetric exchange interactions. *Phys. Rev. B* **2015**, *92*, 224428, doi:10.1103/PhysRevB.92.224428.
14. Khalyavin, D.D.; Salak, A.N.; Manuel, P.; Olekhnovich, N.M.; Pushkarev, A.V.; Radysh, Y.V.; Fedorchenko, A.V.; Fertman, E.L.; Desnenko, V.A.; Ferreira, M.G.S. Antisymmetric exchange in La-substituted $BiFe_{0.5}Sc_{0.5}O_3$ system: Symmetry adapted distortion modes approach. *Z. Krist. Cryst. Mater.* **2015**, *230*, 767–774, doi:10.1515/zkri-2015-1873.
15. Salak, A.N.; Khalyavin, D.D.; Zamaraite, I.; Stanulis, A.; Kareiva, A.; Shilin, A.D.; Rubanik, V.V.; Radyush, Y.V.; Pushkarev, A.V.; Olekhnovich, N.M.; et al. Metastable perovskite $Bi_{1-x}La_xFe_{0.5}Sc_{0.5}O_3$ phases in the range of the compositional crossover. *Phase Transit.* **2017**, *90*, 831–839, doi:10.1080/01411594.2017.1290802.
16. Lu, C.; Hu, W.; Tian, Y.; Wu, T. Multiferroic oxide thin films and heterostructures. *Appl. Phys. Rev.* **2015**, *2*, 021304, doi:10.1063/1.4921545.
17. Martin, L.W.; Chu, Y.H.; Ramesh, R. Advances in the growth and characterization of magnetic, ferroelectric, and multiferroic oxide thin films. *Mater. Sci. Eng. R Rep.* **2010**, *68*, 89–133, doi:10.1016/j.mser.2010.03.001.
18. Yan, F.; Zhu, T.J.; Lai, M.O.; Lu, L. Enhanced multiferroic properties and domain structure of La-doped $BiFeO_3$ thin films. *Scr. Mater.* **2010**, *63*, 780–783, doi:10.1016/j.scriptamat.2010.06.013.
19. Chen, X.; Hu, G.; Yan, J.; Wang, X.; Yang, C.; Wu, W. Enhanced multiferroic properties of (1 1 0)-oriented $BiFeO_3$ film deposited on $Bi_{3.5}Nd_{0.5}Ti_3O_{12}$-buffered indium tin oxide/Si substrate. *J. Phys. D Appl. Phys.* **2008**, *41*, 225402, doi:10.1088/0022-3727/41/22/225402.
20. Zhang, Q.; Sando, D.; Nagarajan, V. Chemical route derived bismuth ferrite thin films and nanomaterials. *J. Mater. Chem. C* **2016**, *4*, 4092–4124, doi:10.1039/C6TC00243A.
21. Deng, X.; Huang, J.; Sun, Y.; Liu, K.; Gao, R.; Cai, W.; Fu, C. Effect of processing parameters on the structural, electrical and magnetic properties of BFO thin film synthesized via RF magnetron sputtering. *J. Alloys Compd.* **2016**, *684*, 510–515, doi:10.1016/j.jallcom.2016.05.114.
22. Deng, X.; Zeng, Z.; Xu, R.; Qin, X.; Li, X.; Wang, Y.; Gao, R.; Wang, Z.; Chen, G.; Cai, W.; et al. Effect of annealing atmosphere on structural and multiferroic properties of $BiFeO_3$ thin film prepared by RF magnetron sputtering. *J. Mater. Sci. Mater. Electron.* **2019**, *30*, 16502–16509, doi:10.1007/s10854-019-02026-0.
23. Hu, C.-W.; Yen, C.-M.; Feng, Y.-C.; Chen, L.-H.; Liao, B.-Z.; Chen, S.-C.; Liao, M.-H. Multi-ferroic properties on $BiFeO_3/BaTiO_3$ multi-layer thin-film structures with the strong magneto-electric effect for the application of magneto-electric devices. *Coatings* **2021**, *11*, 66.
24. Abramov, A.; Alikin, D.; Sobol, A.; Myakishev, D.; Slabov, V.; Trusov, L.; Safina, V.; Turygin, A.; Vasiliev, A.; Shur, V.; et al. Chemical solution deposition of $BiFeO_3$ films with layer-by-layer control of the coverage and composition. *Coatings* **2020**, *10*, 438.
25. Dubourdieu, C.; Kang, S.B.; Li, Y.Q.; Kulesha, G.; Gallois, B. Solid single-source metal organic chemical vapor deposition of yttria-stabilized zirconia. *Thin Solid Film.* **1999**, *339*, 165–173, doi:10.1016/S0040-6090(98)01330-3.
26. Murauskas, T.; Kubilius, V.; Saltyte, Z.; Plausinaitiene, V. Metalorganic chemical vapor deposition and investigation of non-stoichiometry of undoped $BaSnO_3$ and La-doped $BaSnO_3$ thin films. *Thin Solid Film.* **2019**, *692*, 137575, doi:10.1016/j.tsf.2019.137575.
27. Jiang, J.; Shen, W.; Hertz, J.L. Fabrication of epitaxial zirconia and ceria thin films with arbitrary dopant and host atom composition. *Thin Solid Film.* **2012**, *522*, 66–70, doi:10.1016/j.tsf.2012.09.013.
28. Zarkov, A.; Stanulis, A.; Mikoliunaite, L.; Katelnikovas, A.; Jasulaitiene, V.; Ramanauskas, R.; Tautkus, S.; Kareiva, A. Chemical solution deposition of pure and Gd-doped ceria thin films: Structural, morphological and optical properties. *Ceram. Int.* **2017**, *43*, 4280–4287, doi:10.1016/j.ceramint.2016.12.070.
29. Jonauske, V.; Stanionyte, S.; Chen, S.-W.; Zarkov, A.; Juskenas, R.; Selskis, A.; Matijosius, T.; Yang, T.C.K.; Ishikawa, K.; Ramanauskas, R.; et al. Characterization of sol-gel derived calcium hydroxyapatite coatings fabricated on patterned rough stainless steel surface. *Coatings* **2019**, *9*, 334.
30. Gul, E.; Stanulis, A.; Barushka, Y.; Garskaite, E.; Ramanauskas, R.; Morkan, A.U.; Kareiva, A. The influence of thermal processing on microstructure of sol–gel-derived $SrSnO_3$ thin films. *J. Mater. Sci.* **2017**, *52*, 12624–12634, doi:10.1007/s10853-017-1385-y.
31. Karoblis, D.; Griesiute, D.; Mazeika, K.; Baltrunas, D.; Karpinsky, D.V.; Lukowiak, A.; Gluchowski, P.; Raudonis, R.; Katelnikovas, A.; Zarkov, A.; et al. A facile synthesis and characterization of highly crystalline submicro-sized $BiFeO_3$. *Materials* **2020**, *13*, 3035, doi:10.3390/ma13133035.
32. Carranza-Celis, D.; Cardona-Rodríguez, A.; Narváez, J.; Moscoso-Londono, O.; Muraca, D.; Knobel, M.; Ornelas-Soto, N.; Reiber, A.; Ramírez, J.G. Control of multiferroic properties in $BiFeO_3$ nanoparticles. *Sci. Rep.* **2019**, *9*, 3182, doi:10.1038/s41598-019-39517-3.
33. Selbach, S.M.; Einarsrud, M.-A.; Grande, T. On the thermodynamic stability of $BiFeO_3$. *Chem. Mater.* **2009**, *21*, 169–173, doi:10.1021/cm802607p.